

Holographic projection system with programmable control of state of polarization, focus plane and size of the reconstruction

Jeffrey A. Davis,^a Ignacio Moreno,^b Jason P. Sorger,^a María M. Sánchez-López,^{c,*} and Don M. Cottrell^a

^aDepartment of Physics, San Diego State University, San Diego, California 92182-1233, USA

^bDepartamento de Ciencia de Materiales, Óptica y Tecnología Electrónica, Universidad Miguel Hernández, 03202 Elche, Spain

^cInstituto de Bioingeniería, Departamento de Física y Arquitectura de Computadores, Universidad Miguel Hernández, 03202 Elche, Spain

Abstract. A holographic projection system based on the encoding of computer-generated holograms onto a spatial light modulator is discussed. We show how the size, location, and polarization state of the output can be controlled completely electronically, without physically moving any element in the system. It is finally shown that the system is capable to produce optical logical operations by superimposing two different images encoded onto orthogonal polarization states. We show how these images can be added or subtracted, giving a polarization-based logic system. Experimental results are included in all cases.

Keywords: Liquid-crystal displays, Computer-Generated Holograms, Polarization.

*Corresponding Author, E-mail: mar.sanchez@umh.es

1. Introduction

As the resolution of spatial light modulators (SLMs) improves, the capability for encoding computer-generated holograms becomes more practical. Holographic laser projection [1] is one of the multiple applications that will benefit from the development of newer high resolution SLMs since they will provide higher quality image reconstruction. In this technique, a phase-only Fourier transform computer-generated hologram is computed and displayed onto a SLM. The hologram output reconstruction is recovered by optically Fourier transforming the field. A number of works have exploited this approach in combination with the use of three different wavelengths, to provide a large color range in comparison to conventional projectors [2-4].

A requirement usually demanded in projection systems is the capability to focus the image in different planes and with different sizes. For that reason, holographic projector systems incorporate zoom lenses. These can be made with tunable lenses to provide automatic zoom and provide different magnifications without moving elements [5-7], or by using scaled Fresnel transforms as reported in [8].

Another important issue is the control of the state of polarization. For instance, in many 3D applications, the generation of images having different polarizations would be important when using special viewing glasses where each eye detects a different polarization state [9].

In this work, we discuss ways of encoding the Fourier transform of a desired output, the Fourier transform lens, and the output polarization state onto a single SLM. This way we are able to generate a holographic projection system where the state of polarization, and the focusing plane can be controlled at will from the computer, without any moving elements. The two key advances that allow us to achieve such type of control are: 1) an optical system that uses a double pass through a parallel aligned SLM to independently phase-modulate two orthogonal polarization components [10,11] and, 2) a Fourier transform algorithm useful for the fast calculation of diffraction patterns to be displayed onto SLMs [12]. Fresnel diffraction calculations have been applied to design precise computer-generated holograms to be displayed in SLMs [13]. We have previously used the fast calculation of Fresnel diffracted patterns to implement a virtual propagation system [14], where we could experimentally observe the propagation of a light beam without requiring any moving element. Here we extend this approach to achieve automatic control of the focusing plane of the holographic display system without requiring zoom lenses. Then we combine the polarization control to achieve a reconstruction image with controlled state of polarization. Finally, we show polarization-based logic operations based on the subtraction or addition of two polarization images.

2. Review of lens-encoded patterns

Let us begin with a brief review of computer-generated holograms. We use a one-dimensional notation for convenience and consider an input function $g(x)$. Using a computer system, the inverse Fourier transform of this function can be formed as

$$G(\xi) = \mathcal{F}^{-1}\{g(x)\}. \quad (1)$$

Here ξ denotes the spatial frequency. A phase-only function $G(\xi)$ is desirable since it can be directly encoded by the display when the input polarization is linear and parallel to the LC director. However, $G(\xi)$ in Eq. (1) is not in general a phase-only function. It is well-known that keeping only the phase of the Fourier transform of the image and discarding the magnitude results in an edge-enhancement effect [15]. Different techniques exist to avoid this effect. One simple method consists in multiplying the input object to be reconstructed by a random phase pattern [16]. Other techniques involve the use of iterative Fourier transform algorithms [17]. In these cases, the resulting function $G(\xi)$ to be displayed onto the SLM is a phase-only function that reconstructs the desired pattern. However, note that, if required, amplitude and phase can be combined onto a single phase-only SLM using encoding techniques [18,19]. For simplicity, we assume here that $G(\xi)$ is already a phase-only function that can be directly encoded onto the SLM. We achieve this situation simply by selecting input objects that already consist in edges, as it will be shown next in the experiments.

There are two experimental ways of taking the Fourier transform of this function in order to obtain the original input function. One standard way is to place a converging external lens after the SLM. Assuming the lens is placed right behind the SLM and has a focal length F_1 , its corresponding quadratic phase function is represented as $Z^*\{\xi, F_1\} = \exp\{-i\pi\xi^2/\lambda F_1\}$. The Fourier transform of the function $\mathcal{F}\{G(\xi)\} = g(x)$ is formed in the focal plane of the lens. However, the size of the image is also controlled by the focal length F_1 of the lens. So, the size and location of the Fourier transform are determined by the external lens function. Note that ξ represents the spatial frequency of the function $g(x)$. Thus, when $G(\xi)$ is displayed onto an

SLM with $N \times N$ pixels and a pixel size of Δ , the scale of the reconstruction is given proportional to $\lambda F_1 / N \Delta$.

In the second and more versatile approach, the lens function can also be encoded onto the SLM. Here, the pattern encoded onto the SLM consists of the product of the inverse Fourier transform function with the converging lens function as [20]:

$$H(\xi) = Z^*(\xi, F_1)G(\xi) = Z^*(\xi, F_1)\mathcal{F}^{-1}\{g(x)\}. \quad (2)$$

These are called Fourier lens encoded patterns. Note that the pixelated structure of the SLM imposes a limit to the shortest focal length that can be properly displayed in the SLM. This is known as the Nyquist focal length and it is given by $F_N = N\Delta^2/\lambda$ [21], and a recent review of its implications in a zoom lens system was presented in [7]. As before, both the size and location of the output function are determined by the focal length F_1 of the lens. Therefore, if we change the output size, the location where the hologram reconstruction appears also changes.

In a previous work [14], we were able to virtually move the focal plane by forming the Fresnel diffraction of the pattern in Eq. (2). As before, the size of the output will be determined by the focal length of the Fourier transform lens. However, now we can translate the location of the image by a distance d . To accomplish this, the angular spectrum method is applied [22]. In this algorithm, we take the Fourier transform of the function $H(\xi)$ in Eq. (2). Next, we multiply this Fourier transform by a converging lens function whose focal length depends on the propagation distance d , by which we will translate the image location from the original focal point. Finally, we take the inverse Fourier transform of this product. This operation can be written (using the notation in Eq. (2)) as

$$J(\xi) = \mathcal{F}^{-1}\{Z^*(\xi, F_2(d))\mathcal{F}[H(\xi)]\}. \quad (3)$$

Here, the function $Z^*(\xi, F_2(d))$ is a converging lens function whose focal length is given by $F_2 = f^2/d$ where $f = N\Delta^2/\lambda$ is the Nyquist focal length for the Fourier transform performed by the computer, N is the array size, and Δ is the pixel size corresponding to the SLM.

The function $J(\xi)$ thus represents the pattern $H(\xi)$ propagated a distance d from its original location. Therefore, when $J(\xi)$ is displayed onto the SLM, which is kept fixed on in its original position, the result is equivalent to virtually placing the function $H(\xi)$ a distance d from the SLM. Note that, in general, the function $J(\xi)$ is not a phase-only function. However, as we show next, displaying only the phase of this function reproduced very well the expected result with the fully complex function.

Therefore, in this case, the original output function that was formed at a distance F_1 from the SLM can be shifted to a new distance given by $F_1 - d$, without physically moving any element in the system. The virtual location of the hologram has been displaced a distance d from the SLM. But the scale of the Fourier transform is kept fixed, determined by the value of F_1 . Thus, the flexibility of the proposed system includes changing the focal plane, while keeping constant the size of the hologram reconstruction. For computational purposes, this algorithm is much faster than the Fresnel diffraction algorithm because Eq. (3) involves two fast Fourier transform operations [12].

In this work, we present an additional advance of this capability where the polarization state of the output can be controlled. Next, we review our experimental system that allows such polarization control.

3. Generation of computer-generated holograms with designed polarization states

In order to generate an output with a desired polarization state, we use our single SLM system that has been reported previously [10,11] and shown in Fig. 1. We use a transmissive parallel-aligned liquid crystal (LC) SLM manufactured by Seiko Epson with 640x480 pixels having dimensions of $\Delta=42 \mu\text{m}$. The phase shift of each pixel is controlled over 2π radians at the Argon laser wavelength of 514.5 nm. The LC director is

oriented vertically, and therefore the linear vertical polarization component is phase modulated, while the horizontal component is unaffected. The input to the system is selected linearly polarized oriented at 45 degrees to the LCSLM director axis.

The LCSLM screen is divided in two halves, where two different phase patterns are addressed, each with a radius of $N = 120$ pixels, as shown in Fig. 1. The initial beam has vertical and horizontal polarization components A and B as shown in the figure. This beam illuminates the left half part of the screen where a first pattern $G_A(\xi)$, calculated following Eq. (1) is encoded. After the beam is transmitted, the output now consists of electric field components A' and B where the desired pattern is encoded onto the vertical polarization component (A'). The horizontal component (B) is perpendicular to the LC director axis and is unaffected.

Then, by means of a lens (L_2) and a mirror (R), the beam is reflected back to the right part of the LCSLM. The initially vertical and horizontal linearly polarization components are reversed by the insertion of the quarter-wave plate (QWP), oriented at 45 degrees with respect to the LC director axis. Now the horizontal linear polarization component (B), which was not affected by the LCSLM in the initial passage, becomes vertically polarized on the beam illuminating the right side of the LCSLM and will be modulated by the second phase pattern $G_B(\xi)$ encoded on this side of the display. After the beam is transmitted, the output now consists of the desired electric field components B' and A' where both electric field components are now modulated with independent phase-only computer-generated holograms.

Note that the focusing lens and mirror in Fig. 1 comprise a 4f imaging system. Thus, the pattern $G_A(\xi)$ is imaged with unit magnification onto the pattern $G_B(\xi)$, but the initial vertical polarization is converted into the horizontal polarization (and vice versa). As a result, the left side of the SLM encodes one component of the desired output Jones vector $\mathbf{V}(\xi)$, while the right side encodes the other component, i.e.,

$$\mathbf{V}(\xi) = \begin{pmatrix} G_A(\xi) \\ G_B(\xi) \end{pmatrix}. \quad (4)$$

The output beam is directed towards the detector using a non-polarizing beam splitter (NPBS). A polarization analyzer is placed before the detector to verify the polarization properties of the hologram reconstruction.

A physical lens (L_3 in Fig. 1) could be used to obtain the output at the detector, following the first approach previously described in Eq. (1). Alternatively, the lens can be encoded also in the holograms, as the second approach previously mentioned in Eq. (2). Finally, the focusing plane can be shifted longitudinally by applying the propagation algorithm described in Eq. (3).

Next, we provide different experiments demonstrating these possibilities.

4. Experimental results

4.1 Control of the focus plane

In the first experiment, we started with a small smiley face pattern located on the left half of the input screen. We formed the inverse Fourier transform of this and encoded a lens function having a focal length of $F_1 = 50$ cm, to generate a first hologram $H_A(\xi)$ (Eq. (2)) to be displayed on the left part of the SLM screen. We then used the same smiley face pattern located on the right half of the input screen. We again formed the inverse Fourier transform, but now encoded a lens function having a focal length of $F_1 = 75$ cm, to generate the second hologram $H_B(\xi)$ to be displayed on the right part of the SLM screen. We then added the two holograms onto a single pattern that is displayed onto the LCSLM. As mentioned before, the input polarizer is selected at 45° , and therefore the two polarization components, vertical and horizontal, have the same weight, and both patterns are visible. We note that the analyzer is not included in Fig. 1, since here we do not care about the polarization state of the reconstruction.

Figure 2(a) shows the output captured using a camera located a distance of 50 cm from the LCSLM and the smaller smiley face on the left side is focused, while the right pattern is out of focus. We then moved

the camera to a distance of 75 cm. Figure 2(b) shows that now the pattern on the right is in focus, while the pattern on the left one is out of focus. Note how the pattern focused in Fig. 2(b) is larger than the pattern focused in Fig. 2(a), by a factor 1.5 corresponding to the ratio $75/50$ of the corresponding focal lengths.

Next, we applied the Fresnel diffraction procedure to calculate a new hologram $J_A(\xi)$ according to Eq. (3), again with the smaller smiley face pattern and with the same value $F_1 = 50$ cm but shifted by $d = 25$ cm. This new hologram $J_A(\xi)$ is combined with the previous $H_B(\xi)$. Figure 2(c) is the result when the detector is still located a distance of 75 cm from the LCSLM. But now it shows the two patterns in focus. Note that while the location of the smaller smiley face pattern has changed, its size is unchanged.

4.2 Control of the size of the reconstruction

As a second example, we further demonstrate the capability to change the scale without changing the focusing plane. We exploit the above described virtual propagation technique, i.e., no zoom lens is required. The change of the scale of the hologram reconstruction is achieved by changing the focal length F_1 of the Fourier lens encoded on the hologram. But then, the output is placed back into focus in the same original plane by virtually propagating the location of the hologram a distance equivalent to the difference in focal length with respect to the original case.

This is shown in the experimental result in Fig. 3. Here the two patterns displayed on each side of the SLM encode the same hologram, so a single reconstruction is obtained. We select the detector placed at a fixed distance of 70 cm from the LCSLM. However, we use three different focal lengths for the encoded Fourier lens, of $F_1 = 90$ cm, $F_1 = 70$ cm, and $F_1 = 50$ cm, respectively in Fig. 3(a), 3(b) and 3(c). Obviously, the output pattern in Fig. 3(b) appears in focus. In order to obtain also focused outputs in Figs. 3(a) and 3(c), it is required to add a virtual Fresnel propagation

of $d = -20$ cm in Fig. 3(a) and of $d = +20$ cm in Fig. 3(c). Note that the virtual propagation can be of positive or negative distances, as already demonstrated in [14].

The three output reconstructions in Fig. 3 show a different scale due to the different encoded focal length F_1 (the Fresnel propagation does not change the scaling). This approach is therefore completely different to the change in scale achieved by using zoom lenses, as in [5,6].

4.3 Control of the state of polarization

In these previous experiments, we did not place the analyzer shown in Fig. 1, since the polarization state was not a concern. Next, we explore the polarization capabilities of the system.

We again generate two copies of the hologram used in Fig. 3(b), so we simply apply the same pattern to the left and right halves of the LCSLM. This results in an output that is linearly polarized at 45 degrees. Experimental results are shown in Fig. 4(a). The case on the left shows the case without a polarization analyzer. The state of polarization becomes evident when we place six different polarization analyzers – a linear polarizer analyzer oriented at 0, 45, 90, and 135 degrees and both left and right circular analyzers (LCP and RCP). We see that when the linear analyzer is oriented at -45 degrees, the hologram reconstruction is cancelled, indicating that the output is linearly polarized at +45 degrees. For all other analyzers, the full output reconstruction is retrieved.

However, when a phase shift of $\pi/2$ is applied to the pattern on the right side (by uniformly adding the corresponding gray level to this side of the SLM), this results in a circularly polarized output, as shown in Fig. 4(b). Now we observe that the output disappears for the RCP analyzer, while it is fully transmitted for the LCP analyzer. For all linear polarizers the output is visible. This confirms that the hologram reconstruction is right circularly polarized, and confirms the polarization control.

5. Polarization logic

Finally, as a result demonstrating the potential of this system, an example of polarization-based logic operations is shown. We calculate two holograms from two smiling face patterns, but in one of them, the smile is removed. They have the same size and are encoded with the same focal length.

Figure 5 shows the corresponding results when we use linear polarization analyzers. When the analyzers are oriented vertical and horizontal (Fig. 5(a) and Fig. 5(d)), the two patterns used in the holograms design are recovered: the complete smiling face for vertical polarization, and the face without the smile for horizontal polarization.

Figures 5(b) and 5(e) correspond to the orientations of the linear polarization analyzers at +45 degrees and at -45 degrees respectively. In the first case, the result corresponds to the addition of the output reconstructions encoded in each (vertical and horizontal) polarization components. Figure 5(c) illustrates a diagram showing the addition operation. The outputs are encoded onto vertical and horizontal components of the electric field (vectors B' and A' respectively). These vectors project equally to the analyzer transmission axis when it is oriented at +45 degrees (resulting in the corresponding output vectors b' and a'). Therefore, the addition of the two contributions is produced.

This is not the case when the analyzer is oriented at -45 degrees, as Fig. 5(f) illustrates. Now the vertical and horizontal electric fields project to the orientation of the analyzer transmission axis in opposition, thus resulting in a subtraction operation. This is equivalent to the well-known operation of magneto-optic devices as binary phase-only modulators [23]. The output is now shown in Fig. 5(d), where only the difference between the two encoded outputs is observed, i.e., the smile.

6. Conclusions

In summary, we have experimentally demonstrated a proof-of-concept of a holographic projection system that combined two interesting features: 1) programmable control of the focusing plane and size of the reconstruction, and 2) programmable control of the state of polarization of the hologram reconstruction.

The first feature is achieved thanks to the application of a technique [14], where the hologram plane is virtually propagated using a using Fresnel propagation algorithm, while being displayed in the same SLM. Using a previously reported angular spectrum algorithm [12] that allows fast calculations of the Fresnel propagated versions of the hologram. We have shown that this technique allows control of the axial position of the output reconstruction without changing the size. We have also shown that the technique also allows changing the size of the output reconstruction while keeping a fixed focusing plane. Note that this is fully achieved by encoding the Fourier transform lens function and the virtual displacement on the hologram displayed on the SLM, without requiring any additional zoom lens.

The second feature, the polarization control, is achieved by using an optical system with a double pass through a LCSLM [10,11]. Two independent holograms can be displayed on each side of the SLM to control two orthogonal polarization components. This way we can apply the previously described Fourier encoded holograms to two independent patterns and provide a programmable control of the state of polarization of the holographic projection output. This can be an interesting property for 3D patterns visualization, where two images with orthogonal polarizations are required. Here, as an example, we have provided a demonstration of polarization-based logical operations, where the addition and subtraction of two images encoded on the two orthogonal linear polarizations is shown.

We finally want to indicate some technological aspects where the system used here for demonstration could be adapted and made compact for practical application. First, note that the double-pass geometry in Fig. 1 implies the use of a beam-splitter, with the subsequent loss of power. Additionally this geometry forces us to divide the SLM screen in two parts, thus reducing the available space bandwidth and enlarging

the Nyquist focal length limit. This could be avoided simply using in cascade two transmissive SLMs as the prototype one used here. However, the SLM industry has moved to reflective liquid-crystal on silicon (LCOS) devices, with various newer high-resolution displays. An optical system similar to that in Fig. 1 can be built with LCOS-SLMs [24]. But since these are reflective devices, two beam-splitters would be required with substantial loss in intensity. Alternatively, LCOS-SLMs can be used with an angle, but then the system cannot be compact because requires enough room to separate the input and the reflected beam. We consider that the development of high-resolution transmissive parallel-aligned liquid-crystal SLMs could be of great interest for the practical implementation of the proposed technique, as well as for many others.

Acknowledgements: IM and MMSL acknowledge financial support from Ministerio de Economía y Competitividad from Spain and FEDER Funds (ref. FIS2015-66328-C3-3-R) and from Conselleria d'Educació, Investigació, Cultura i Esport, Generalitat Valenciana (ref. PROMETEO-2017-154).

References

- [1]. E. Buckley, "Holographic laser projection," *J. Displ. Technol.* **7**(13), 135-140 (2011).
- [2]. M. Makowski, I. Ducin, M. Sypek, A. Siemion, A. Siemion, J. Suszek, and A. Kolodziejczyk, "Color image projection based on Fourier holograms," *Opt. Lett.* **35**(8), 1227-1229 (2010).
[<https://doi.org/10.1364/OL.35.001227>]
- [3]. A. Jesacher, S. Bernet, and M. Ritsch-Martel, "Colour hologram projection with an SLM by exploiting its full phase modulation range," *Opt. Express* **22**(17), 20530-20541 (2014).
[<https://doi.org/10.1364/OE.22.020530>]
- [4]. J. Hecht, "Cutting-edge cinema," *Opt. & Photon. News* **29**(6), 28-35 (2018).

- [5]. H.-C. Lin, N. Collings, M.-S. Chen, and Y.-H. Lin, "A holographic projection system with an electrically tuning and continuously adjustable optical zoom," *Opt. Express* **20**(25), 27222-27229 (2012). [<https://doi.org/10.1364/OE.20.027222>]
- [6]. M.-S. Chen, N. Collings, H.-C. Lin, and Y.-H. Lin, "A holographic projection system with an electrically adjustable optical zoom and a fixed location of zeroth-order diffraction," *J. Displ. Technol.* **10**(6), 450-455 (2014).
- [7]. J. A. Davis, T. I. Hall, I. Moreno, J. P. Sorger, D. M. Cottrell, "Programmable zoom lens system with two spatial light modulators: Limits imposed by the spatial resolution," *Appl. Sci.* **8**(6), 1006 (2018). [<https://doi.org/10.3390/app8061006>]
- [8]. T. Shimobaba, M. Makowski, T. Kakue, M. Oikawa, N. Okada, Y. Endo, R. Hirayama, and T. Ito, "Lensless zoomable holographic projection using scaled Fresnel diffraction," *Opt. Express* **21**(21), 25285-25290 (2013). [<https://doi.org/10.1364/OE.21.025285>]
- [9]. A. J. Woods, "Crosstalk in stereoscopic displays: a review", *J. Electron. Imaging* **21**(4), 040902 (2012). [<https://doi.org/10.1117/1.JEI.21.4.040902>]
- [10]. I. Moreno, J.A. Davis, T.M. Hernandez, D.M. Cottrell, and D. Sand, "Complete polarization control of light from a liquid crystal spatial light modulator," *Opt. Express* **20**(1), 364-376 (2012). [<https://doi.org/10.1364/OE.20.000364>]
- [11] J. A. Davis, I. Moreno, M. M. Sánchez-López, K. Badham, J. Albero, and D. M. Cottrell, "Diffraction gratings generating orders with selective states of polarization," *Opt. Express* **24**(2), 907-917 (2016). [<https://doi.org/10.1364/OE.24.000907>]
- [12]. J. A. Davis and D. M. Cottrell, "Ray matrix analysis of the fast Fresnel transform with applications towards liquid crystal displays," *Appl. Opt.* **51**(5), 644-650 (2012).

- [<https://doi.org/10.1364/AO.51.000644>]
- [13]. J. Liang and M. F. Becker, “Spatial bandwidth analysis of fast backward Fresnel diffraction for precise computer-generated hologram design,” *Appl. Opt.* **53**(27), G84-G94 (2014).
[<https://doi.org/10.1364/AO.53.000G84>]
- [14]. J. A. Davis, I. Moreno, D. M. Cottrell, C. A. Berg, C. L. Freeman, A. Carmona, W. Debenham, “Experimental implementation of a virtual optical beam propagator system based on a Fresnel diffraction algorithm,” *Opt. Eng.* **54**(10), 103101 (2015).
[<https://doi.org/10.1117/1.OE.54.10.103101>]
- [15]. J. L. Horner and P. D. Gianino, “Phase-only matched filtering,” *Appl. Opt.* **23**(6), 812-816 (1984).
[<https://doi.org/10.1364/AO.23.000812>]
- [16]. J. A. Davis, S. W. Flowers, D. M. Cottrell, and R. A. Lilly, “Smoothing of the edge-enhanced impulse response from binary phase-only filters using random binary patterns,” *Appl. Opt.* **28**, 2987-2988 (1989). [<https://doi.org/10.1364/AO.28.002987>]
- [17]. F. Wyrowski, “Diffractive optical elements: iterative calculation of quantized, blazed phase structures,” *J. Opt. Soc. Am. A* **7**(6), 961–969 (1990). [<https://doi.org/10.1364/JOSAA.7.000961>]
- [18]. J. A. Davis, D. M. Cottrell, J. Campos, M. J. Yzuel, I. Moreno, “Encoding amplitude information onto phase-only filters,” *Appl. Opt.* **38**(23), 5004-5013 (1999).
[<https://doi.org/10.1364/AO.38.005004>]
- [19]. T. W. Clark, R. F. Offer, S. Franke-Arnold, A. S. Arnold, and N. Radwell, “Comparison of beam generation techniques using a phase only spatial light modulator,” *Opt. Express* **24**(6), 6249–6264 (2016). [<https://doi.org/10.1364/OE.24.006249>]
- [20]. J. A. Davis, D. M. Cottrell, R. A. Lilly and S. W. Connely, “Multiplexed phase-encoded lenses written on programmable spatial light modulators,” *Opt. Lett.* **14**, 420-422 (1989).

[\[https://doi.org/10.1364/OL.14.000420\]](https://doi.org/10.1364/OL.14.000420)

[21]. J. A. Davis, M. A. Waring, G. W. Bach, R. A. Lilly and D. M. Cottrell, “Compact optical correlator design,” *Appl. Opt.* **28**, 10-11 (1989). [<https://doi.org/10.1364/AO.28.000010>]

[22]. J. W. Goodman, *Introduction to Fourier Optics*, McGraw Hill (1969).

[23]. J. A. Davis, M. A. Waring, “Contrast ratio improvement for the two-dimensional magneto-optic spatial light modulator,” *Appl. Opt.* **31**(29), 6183-6185 (1992).

[\[https://doi.org/10.1364/AO.31.006183\]](https://doi.org/10.1364/AO.31.006183)

[24]. X. Zheng, A. Lizana, A. Peinado, C. Ramírez, J. L. Martínez, A. Márquez, I. Moreno, J. Campos, “Compact LCOS-SLM based polarization pattern beam generator”, *J. Lightwave Technol.* **33**(10), 2047-2055 (2015). [<https://doi.org/10.1109/JLT.2015.2395256>]

Figure Captions

Fig. 1. Double-pass system to generate polarization phase-only computer-generated holograms. The physical lens L_3 can be removed and encoded onto the SLM.

Fig. 2. Experimental demonstration of control of the focusing plane. Fourier lens encoded holograms are designed with focal lengths of $F_1 = 50$ cm (left) and $F_1 = 75$ cm (right). (a) Output at 50 cm from the SLM. (b) Output at 75 cm from the SLM. (c) Output at 75 cm when the left hologram is Fresnel propagated by a distance $d = 25$ cm.

Fig. 3. Experimental demonstration of control of the size of the reconstruction. Detector is fixed, placed at a distance of 70 cm. The focal lengths of the encoded Fourier lens and virtual propagation distances are adjusted to keep a constant focus plane: (a) $F_1 = 90$ cm and $d = -20$ cm. (b) $F_1 = 70$ cm and $d = 0$ cm. (c) $F_1 = 50$ cm and $d = +20$ cm.

Fig. 4. Experimental demonstration of control of the state of polarization. (a) Output linearly polarized at 45 degrees. (b) Output circularly polarized. Analyzers are indicated on each image.

Fig. 5. Polarization logic: A' and B' denote the electric field orientations where the two holograms are encoded. a' and b' indicate the electric field orientations after the analyzer when oriented at ± 45 degrees. (a)-(d) Experimental outputs for linear analyzers oriented vertical, at +45 degrees, horizontal, and at -45 degrees. Diagrams showing the projections of the electric fields in the cases of (e) addition and (f) subtraction of images.

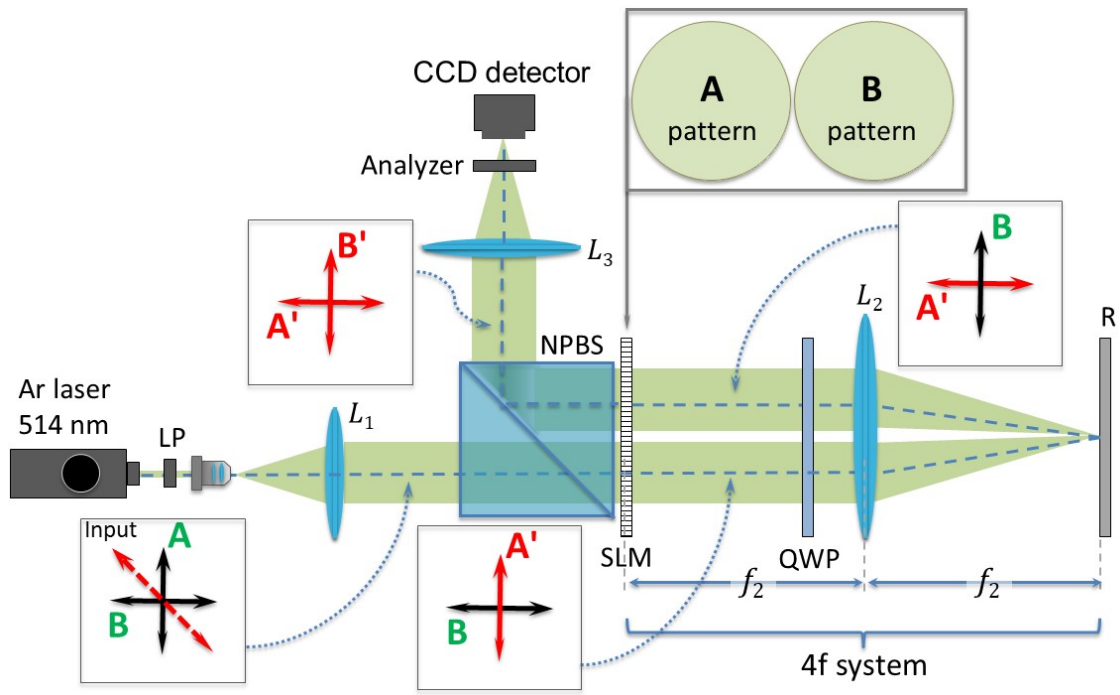


Fig. 1

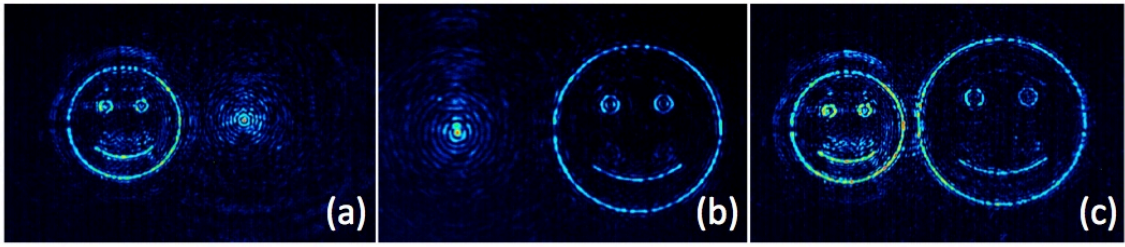


Fig. 2

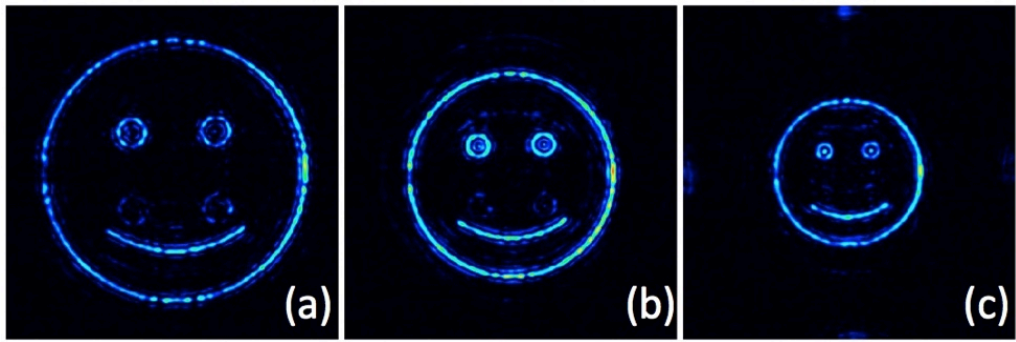


Fig. 3

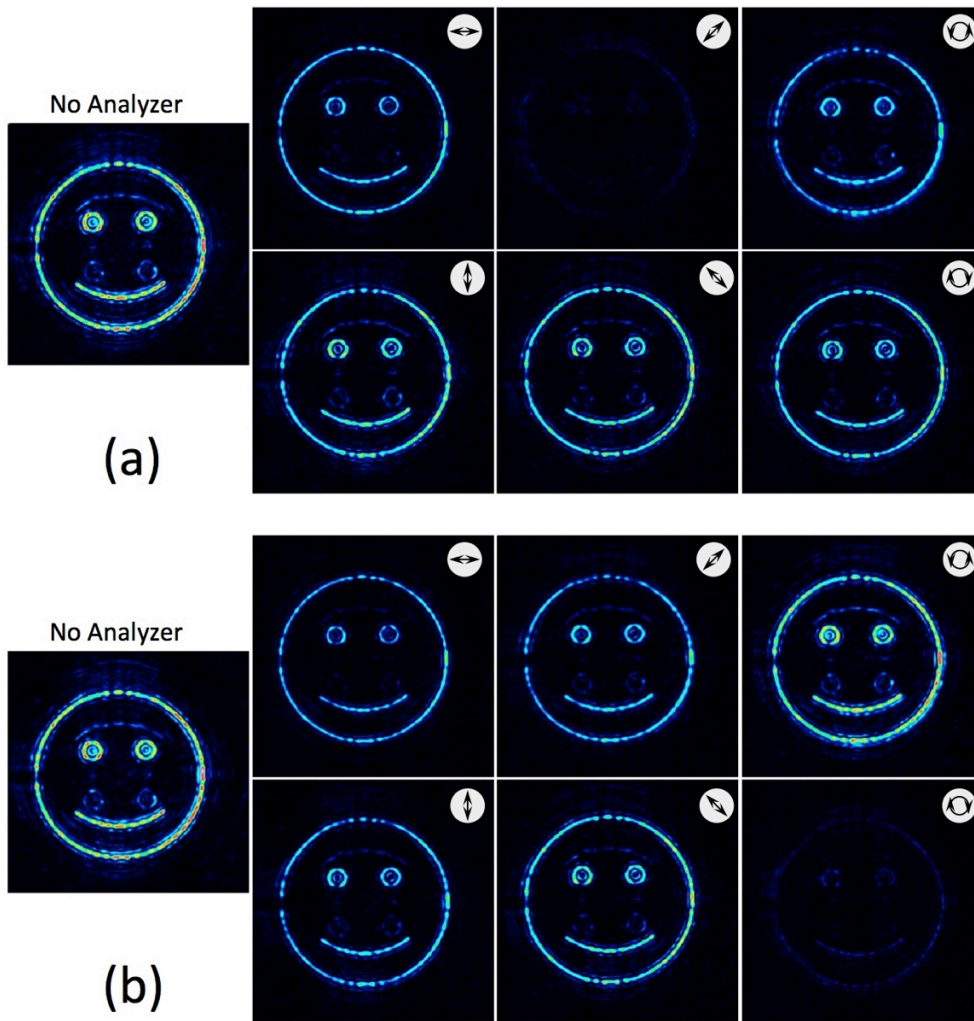


Fig. 4

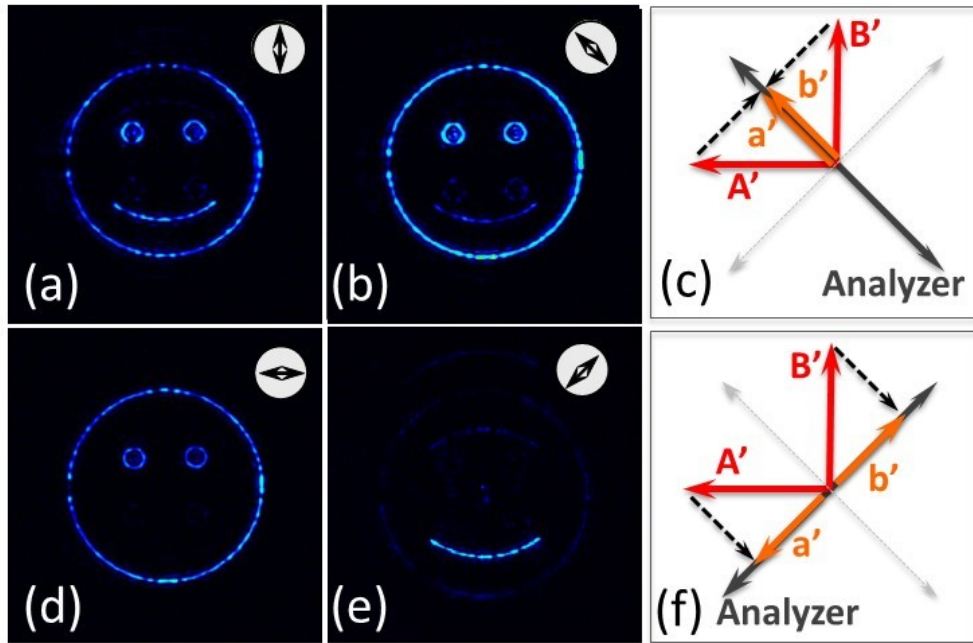


Fig. 5